Rapid Communications

Quantum dynamics of hydrogen in the iron-based superconductor $LaFeAsO_{0.9}D_{0.1}$ measured with inelastic neutron spectroscopy

Jun-ichi Yamaura,[1,*] Haruhiro Hiraka,[2,†] Soshi Iimura,[3] Yoshinori Muraba,[1] Joonho Bang,[1] Kazuhiko Ikeuchi,[4] Mitsutaka Nakamura,[5] Yasuhiro Inamura,[5] Takashi Honda,[2] Masatoshi Hiraishi,[2] Kenji M. Kojima,[2] Ryosuke Kadono,[2] Yoshio Kuramoto,[2,6] Youichi Murakami,[1,2] Satoru Matsuishi,[1] and Hideo Hosono[1,3]

[1]*Materials Research Center for Element Strategy, Tokyo Institute of Technology, Yokohama, Kanagawa 226-8503, Japan*
[2]*Condensed Matter Research Center, Institute of Materials Structure Science, KEK, Tsukuba, Ibaraki 305-0801, Japan*
[3]*Laboratory for Materials and Structures, Tokyo Institute of Technology, Yokohama, Kanagawa 226-8503, Japan*
[4]*Comprehensive Research Organization for Science and Society, Tokai, Ibaraki 319-1106, Japan*
[5]*J-PARC Center, Japan Atomic Energy Agency, Tokai, Ibaraki 319-1195, Japan*
[6]*Department of Physics, Kobe University, Kobe, Hyogo 657-8501, Japan*

(Received 10 November 2018; revised manuscript received 8 May 2019; published 13 June 2019)

Inelastic neutron scattering was performed for an iron-based superconductor $LaFeAsO_{0.9}D_{0.1}$, where most of D (deuterium) replaces oxygen, while a tiny amount goes into the interstitial sites. By first-principles calculation, we characterize the interstitial sites for D (and for H slightly mixed) with four equivalent potential minima. Below the superconducting transition temperature $T_c = 26$ K, excitations emerge in the range 5–15 meV, while they are absent in the reference system $LaFeAsO_{0.9}F_{0.1}$. The strong excitations at 14.5 and 11.1 meV broaden rapidly around 15 and 20 K, respectively, where each energy becomes comparable to twice the superconducting gap. The strong excitations are ascribed to a quantum rattling, or a band motion of hydrogen, which arises only if the number of potential minima is larger than two.

DOI: 10.1103/PhysRevB.99.220505

The discovery of iron-based superconductors has stimulated a growing body of research [1–4]. To identify the mechanism of superconductivity, one needs detailed information about the superconducting gap, together with its temperature dependence. In addition to thermodynamic and transport studies, direct measurements of the energy gaps have been tried by various methods such as photoemission [5,6], tunneling [7], point-contact [8,9], and infrared [10,11] spectroscopies. These methods require a high-quality sample, which is not feasible in some iron-based superconductors made with an intricate procedure of synthesis. Therefore, a direct method is needed that is also applicable to polycrystalline samples with rough surfaces, magnetic impurities, and other imperfections.

Here, we propose a method for the direct detection of the superconducting gap in an iron-based superconductor via coupling to the hydrogen motion at interstitial sites. When two or more interstitial sites of hydrogen are close, the overlap of wave functions causes the splitting of the hydrogen energy levels [12,13]. This quantum phenomenon is known as tunneling splitting, and has long been studied in conventional superconductors by inelastic neutron scattering (INS) [12,14–16]. The magnitudes of the tunneling splitting in known cases are much smaller than the characteristic value of the superconducting gap. As we shall demonstrate, the hydrogen vibration in iron-based superconductors is highly anharmonic at the interstitial sites. Accordingly, generalized tunneling splitting has an exceptionally large energy of the order of 10 meV, which is comparable to the superconducting gap. Hence, the hydrogen motion serves as a good probe for superconductivity. Since the local dynamics is not much influenced by the sample quality, the hydrogen probe has a unique advantage over conventional spectroscopies.

We performed INS measurements for a deuterated $LaFeAsO_{0.9}D_{0.1}$ with $T_c = 26$ K [17]. We found strong intensities in the excitation range of 4–15 meV below T_c. The source of these excitations is ascribed to hydrogen since the reference material $LaFeAsO_{0.9}F_{0.1}$, with the same electronic/magnetic phase diagram [1,17], does not show the corresponding intensities. Throughout this Rapid Communication, we use the term "hydrogen" for both ^{1}H and ^{2}H, and protium (H) or deuterium (D) to distinguish the isotopes explicitly.

We prepared a powder sample of $LaFeAsO_{0.9}D_{0.1}$ (D sample), weighing ~30 g, under high pressure [17]. Hydrogen anions (D^-) were substituted for O^{2-} anions [18,19]. In addition, owing to a tiny amount of H in the deuterated reagents [20], some mixture of H at the hydrogen sites is inevitable. Their cross sections σ_{inc} of incoherent scattering are $\sigma_{inc}(H) = 80.3 \times 10^{-24}$ cm^2 and $\sigma_{inc}(D) = 2.1 \times 10^{-24}$ cm^2. The H/D concentration ratio was estimated to be ~0.02 based on the analysis of excitations at 70–130 meV of H and D confined in the O sites (see Supplemental Material [21]). We also prepared $LaFeAsO_{0.9}F_{0.1}$ (F sample) with ~20 g under ambient pressure as the reference for the D sample.

The INS intensities for the D and F samples were measured on a chopper spectrometer (4SEASONS) [22] at BL01 in the pulsed-neutron source at the Japan Proton Accelerator

*jyamaura@mces.titech.ac.jp
†Present address: Korea Atomic Energy Research Institute, Daejeon, Korea; hiraka@kaeri.re.kr

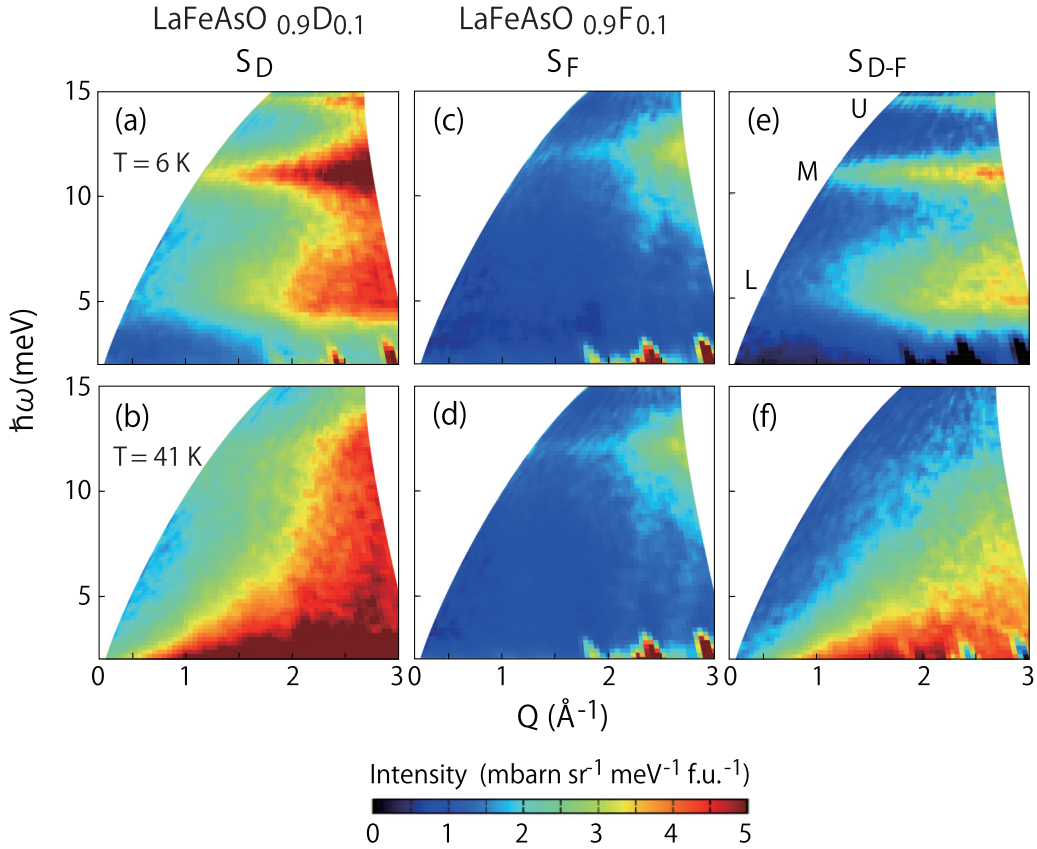

FIG. 1. Color plots of $S_A(Q, \hbar\omega)$ with A = D, F, and D − F at 6 K (a), (c), (e), and 41 K (b), (d), (f). The incident neutron energy is $E_i = 17.5$ meV. (a), (b) S_D from $LaFeAsO_{0.9}D_{0.1}$; (c), (d) S_F from $LaFeAsO_{0.9}F_{0.1}$; (e), (f) the difference map S_{D-F}. U, M, and L in (e) signify the upper, middle, and lower modes, respectively.

Research Complex (J-PARC) in the Materials and Life Science Experimental Facility (MLF). Data were collected at incident neutron energies of $E_i = 9.3$, 17.5, and 44.5 meV [23]. The Fermi-chopper frequency was set to 150 Hz, with a resolution $\hbar\Delta\omega/E_i$ of ∼2% at the energy transfer $\hbar\omega \approx 14$ meV. The time-of-flight data from position-sensitive detectors were converted into the $\boldsymbol{Q}$-angle average $\langle S(\boldsymbol{Q}, \hbar\omega)\rangle_{\text{angle}}$ of the dynamical structure factor by the UTSUSEMI program [24]. We use the notation $S(Q, \hbar\omega)$ for the angle average.

Figure 1 shows $S(Q, \hbar\omega)$ for the D and F samples, written as S_D and S_F, respectively, together with their difference S_{D-F}. Comparing S_D at 6 K below T_c [Fig. 1(a)] and at 41 K above T_c [Fig. 1(b)], we find three groups of excitations at 6 K, all of which are insensitive to Q but merge into a broad feature at 41 K with a strong diffusive character over the entire energy range. In sharp contrast to S_D, the results S_F for the F sample exhibit neither flat excitations at 6 K [Fig. 1(c)] nor diffuse scattering at 41 K [Fig. 1(d)]. Instead, a small temperature-insensitive feature is visible at $\hbar\omega \approx 12$ meV in Figs. 1(c) and 1(d). This is ascribed to phonon scattering as previously reported for the F sample [25]. On the other hand, the magnetic scattering reported at $Q \approx 1.1$ Å [26,27] is not visible at the present scale because of their weak intensities.

Figures 1(e) and 1(f) display the difference map $S_{D-F} \equiv S_D - S_F$ at 6 and 41 K, respectively. At 6 K, the three distinct features are assigned as U, M, and L, as indicated in Fig. 1(e). The D and F samples have almost the same electric and superconducting properties [17]. Consequently, the strong excitations in S_{D-F} must originate from hydrogen.

Figures 2(a) and 2(b) display the energy spectra of S_{D-F} at 6 and 23.5 K, respectively, with $Q = 2.15 \pm 0.15$ Å^{-1}. For each temperature, the scattering peaks are fitted by a Lorentzian spectrum with a linewidth $\hbar\Gamma_\alpha(T)$ where α represents either the U or M mode. Figure 2(c) plots the temperature dependence of $\hbar\Gamma_\alpha(T)$, which shows that both $\hbar\Gamma_U$ and $\hbar\Gamma_M$ barely depend on temperature for $T < 15$ K. A rapid increase is seen however around 20 K, and then both linewidths are weakly temperature dependent as the temperature approaches $T_c \sim 26$ K. In contrast, each peak position $\hbar\omega_\alpha$ is nearly constant against temperature, as shown in Fig. 2(d).

It is likely that the rapid increase of $\hbar\Gamma_\alpha$ at $T \lesssim T_c$ is related to the coupling of the hydrogen motion to electronic excitations. Namely, with increasing temperature toward T_c, the superconducting gap $\Delta(T)$ decreases so as to satisfy the condition $\hbar\omega_\alpha > 2\Delta(T)$. This means that S_{D-F} serves as a probe of the superconducting gap. For comparison, we refer to the INS spectra in $Nb(OH)_x$ ($x \approx 0.002$), where an inelastic peak at ∼0.2 meV below $T_c = 9.2$ K merges into the broad quasielastic feature above T_c [28]. The origin of the peak has been assigned to the tunneling splitting of the interstitial hydrogen in the double-well potential. In contrast to the present case, the inelastic peak in $Nb(OH)_x$ is much smaller than $2\Delta_0 \sim 3$ meV in the system. The peak width below T_c

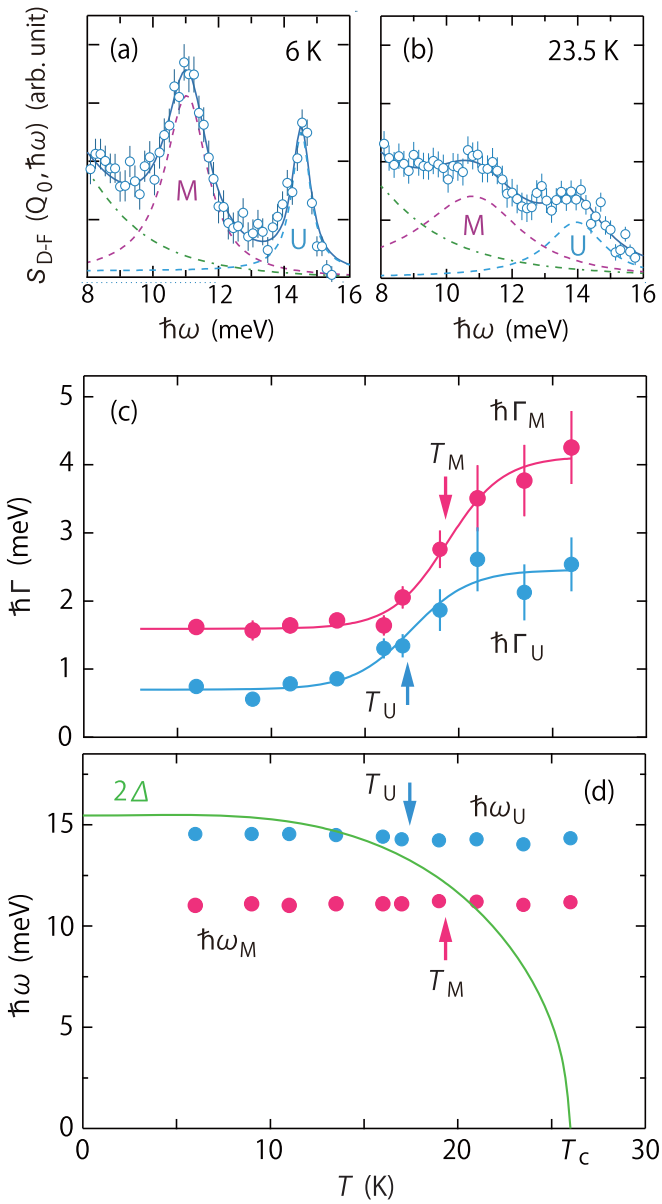

FIG. 2. Scattering intensities with incident neutron energy $E_i = 17.5$ meV at (a) 6 K and (b) 23.5 K for $Q_0 = 2.15 \pm 0.15$ Å^{-1}. The indigo solid line represents the sum of all components, the blue dashed line the U component, the red dashed line the M component, and the green dashed-dotted line the tail of the L component which works as a baseline for M and U components. Also shown are the temperature dependence of (c) the linewidth $\hbar\Gamma_\alpha$ with $\alpha = $ U, M and (d) the peak position $\hbar\omega_\alpha$ for the U and M modes. The blue and magenta solid lines are the results on fitting the U and M peaks, respectively. The green solid line shows the temperature dependence of the BCS gap function $2\Delta(T)$. The arrows indicate the temperature T_α corresponding to the midpoint of $\hbar\Gamma_\alpha(T)$ as fitted by the sigmoid function.

decreases toward the resolution limit upon cooling [28,29]. The change in width is interpreted in terms of a Korringa-type relaxation due to the conduction electrons, which becomes active as the superconducting gap decreases [14,15,28,30].

It appears from Fig. 2(c) that each peak width saturates at both low and high temperatures. We then use the sigmoid function to fit $\hbar\Gamma_\alpha(T)$, as presented in Fig. 2(c). Next, with a trial value for the superconducting gap Δ_0 at zero temperature, we plot $2\Delta(T)$ according to the temperature dependence in BCS theory. For the value $\Delta_0 = 7.8 \pm 0.7$ meV, the midpoint temperatures T_α of both U and M modes agree reasonably well with the relation $\hbar\omega_\alpha = 2\Delta(T_\alpha)$ [Fig. 2(d)]. The estimated gap gives the ratio $2\Delta_0/k_B T_c = 7.0$, which characterizes this compound as a strong-coupling superconductor. According to the point-contact spectra on $LaFeAsO_{0.9}F_{0.1}$ [9], two gaps have been reported, $\Delta_1 \approx 7.9$ meV and $\Delta_2 \approx 2.8$ meV, both of which show a strong deviation from the BCS-like temperature dependence. On the other hand, another experiment on $SmFeAsO_{0.85}F_{0.15}$ [8] with $T_c \sim 42$ K has reported a single gap around 7 meV that shows a BCS-like temperature dependence. The present result for Δ_0 corresponds to the value Δ_1 in Ref. [9], but with a BCS-like temperature dependence. Further study is necessary to reconcile these conflicting observations.

The crossing of $\hbar\omega$ and $2\Delta(T)$ is analogous to the optical threshold in the BCS superconductor [31]. With the finite damping of quasiparticles and/or the presence of a normal component of electrons, the optical conductivity becomes already finite [10,11,32] for $\hbar\omega < 2\Delta_0$ in contrast with the ideal BCS case. In such a case, the midpoint of the increasing conductivity as a function of $\hbar\omega$ corresponds to the relation $\hbar\omega = 2\Delta_0$. The finite damping should also be present in the hydrogen excitations. Hence, the midpoint of $\hbar\Gamma_\alpha(T)$ seems to be a reasonable choice for extracting $2\Delta(T)$.

We proceed to consider the microscopic origin of the observed excitations. First, to investigate the stable positions of the interstitial hydrogen, we performed first-principles calculations using the Vienna *ab initio* simulation package, which is combined with a generalized gradient approximation using the Perdew-Burke-Ernzerhof exchange-correlation function [33]. The cutoff energy for the plane wave is set to 400 eV, and the k-point $3 \times 3 \times 3$ mesh is sampled in the first Brillouin zone. Interstitial hydrogens are placed in a periodically repeated $2 \times 2 \times 1$ supercell corresponding to the interstitial hydrogen number $1/8$ per unit cell. The interstitial hydrogen frequently induces displacements of the surrounding atoms from their equilibrium positions, and forms a self-trapped state [34–36]. However, it has been discussed that thermal fluctuations recover an equivalent level for all interstitial sites, which enables the tunneling [37,38]. There is no consistent microscopic theory on how quantum tunneling occurs at low enough temperatures where thermal fluctuations are negligible. In view of this situation, the calculation was mainly performed using fixed positions of the atoms. In the Supplemental Material, we discuss how the relaxation of the surrounding atoms influences the result. To simulate the system with implanted hydrogen, we place a static point charge at location $\boldsymbol{r}$ in the supercell together with a neutralizing electron. Then, we compute the total energy $E(\boldsymbol{r})$ per supercell, which is minimized at the optimal position $\boldsymbol{r}$ of the positive charge. We define the effective potential for a positive charge, $\Delta E(\boldsymbol{r}) = E(\boldsymbol{r}) - E_0 - \mu$, where E_0 is the corresponding energy without the positive charge, and μ is the chemical potential. As a result, the dynamics of protons or deuterons are neglected in the present simulation.

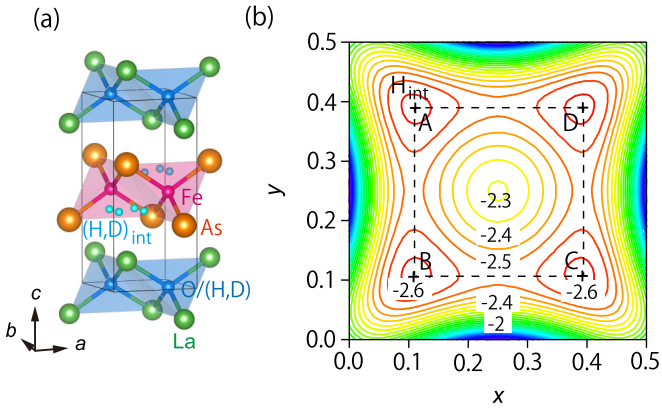

FIG. 3. (a) Crystal structure of $LaFeAsO_{0.9}D_{0.1}$ with the interstitial site H_{int}. (b) Contour map of ΔE in units of eV on the xy plane at $z = 0.425$. The four potential minima marked by the crosses are located at $(0.11, 0.11, 0.425)$ and the equivalent positions. The fourfold rotational axis runs along the line $(0.25, 0.25, z)$. The coordinates are described by the crystallographic units.

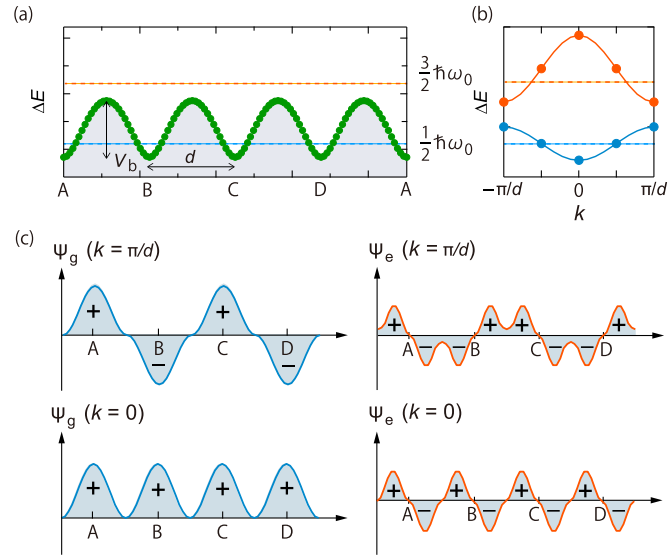

FIG. 4. (a) The line profiles of ΔE through the minima A-B-C-D-A on $z = 0.425$. The tunneling distance d and the potential barrier V_b between the minima are indicated. The blue dashed line represents the ground state in the single harmonic potential at $\frac{1}{2}\hbar\omega_0$, while the orange dashed line represents the first excited state at $\frac{3}{2}\hbar\omega_0$. (b) The blue line shows the spectrum of the tunneling splitting, while the orange line shows that of the highly anharmonic phonons described as quantum rattling. (c) Schematic picture of hydrogen wave functions. Ψ_g stems from the ground state of the harmonic oscillator with $n = 0$, while Ψ_e stems from $n = 1$. The wave functions at neighboring sites have either the same phase ($k = 0$), or opposite phase ($k = \pi/d$).

According to the structure analysis (see Supplemental Material), $LaFeAsO_{0.9}D_{0.1}$ has a ZrCuSiAs-type structure with alternating stacks of conducting $FeAs_4$ and insulating $(O, D)La_4$ layers [Fig. 3(a)]. Figure 3(b) illustrates the contour map of $\Delta E(\boldsymbol{r})$ on the xy plane at $z = 0.425$. Four potential minima appear in $\Delta E(\boldsymbol{r})$ at $\boldsymbol{r} = (0.11, 0.11, 0.425)$ and the crystallographically equivalent positions related by the fourfold rotational symmetry, labeled H_{int} hereafter. The minima are located within the As_5La void with a H_{int}-As distance of 2.15 Å. A Bader charge analysis gives the charge of hydrogen at H_{int} to be 1.33, which implies the interstitial hydrogen lies in hydride [39].

Using the effective potential $\Delta E(\boldsymbol{r})$, we now consider the dynamics of the interstitial hydrogen. Figure 4(a) illustrates the line profile through the minima A-B-C-D-A, as indicated in Fig. 3(b). This corresponds to the pathway of hydrogen migration. The profile features a periodic potential with a tunneling distance $d = 1.13(1)$ Å and potential barrier $V_b = 102$ meV at the saddle point. In the harmonic approximation for the sinusoidal potential, the angular frequency ω_0 is given by $\omega_0^2 = 2\pi^2 V_b/(md^2)$, where m is the isotope mass. Next, we obtain $\hbar\omega_{0,H} = 81$ meV for H and $\hbar\omega_{0,D} = 57$ meV for D. The V_b is comparable to the 80 meV estimated for $Nb(OH)_x$ with $d = 1.17$ Å and $\hbar\omega_0 = 107$ meV [30].

The cross section σ_{inc} of incoherent scattering is much larger in H than D, with the ratio $\sigma_{inc}(H)/\sigma_{inc}(D) \approx 40$. Considering the concentration ratio $n_H/n_D \approx 0.02$, the scattering intensities from the two isotopes should be comparable. Hence, we assume that the features U and M come from the interstitial H and D, respectively. The ratio $\omega_U/\omega_M \approx 1.3$ is rather close to the square root of the atomic mass ratio $\sqrt{m_D/m_H} = \sqrt{2}$. This might be regarded as the isotope effect for harmonic phonons. In fact, for H or D substituting oxygen, the Supplemental Material demonstrates the isotope effect with a reasonable agreement between the calculation and the experimental observation in the range of 70–130 meV. However, since $\hbar\omega_U$ and $\hbar\omega_M$ are much smaller (< 20 meV), it is difficult to ascribe U and M to ordinary vibrations of hydrogen.

We now check the possibility of whether ω_U and ω_M may come from the tunneling motion of hydrogen. The magnitude of the tunneling splitting is sensitive to the distance and mass of the isotopes [12,14,40]. For example, the tunneling splittings are reported as 0.2 meV (H) and 0.02 meV (D) for Nb [28,40], while 6.3 meV (H) and 1.6 meV (D) for α-Mn [41]. The latter values are referred to as giant tunneling splittings, and are caused by the very short tunneling distance of 0.68 Å. The mass of the isotopes affects the tunneling splittings $\omega_{H,D}$ more strongly than the case for phonons, as seen in $\omega_H/\omega_D \approx 10$ for Nb [28,40] and $\omega_H/\omega_D \approx 4$ for α-Mn [41]. Thus, the present value $\omega_U/\omega_M \approx 1.3$ is not consistent with the identification of tunneling splitting.

We therefore propose that the excitations at $\hbar\omega_U$ and $\hbar\omega_M$ are associated with a different type of extremely anharmonic phonons, which can be appropriately called quantum rattling. In this process, the potential barrier is so low that the ordinary excited state, corresponding to the energy $\frac{3}{2}\hbar\omega_0$ in the harmonic case, is actually extended along the pathway connecting the four potential minima, as illustrated in Fig. 4(a). In the four potential minima system, the eigenstates are characterized by the wave numbers $k = 0, \pm\pi/(2d)$, and $\pm\pi/d$, as shown in Fig. 4(b). In addition, the eigenstates are related to the superposition of localized phonons, which have energies $(n + 1/2)\hbar\omega_0$ with $n = 0, 1, \ldots$. Figure 4(c) illustrates the wave functions Ψ_g stemming from $n = 0$, and Ψ_e stemming from $n = 1$. The exact solution of the Schrödinger equation is obtained in terms of the Mathieu functions (see Supplemental Material). If we assign $\hbar\omega_M = 11.1$ meV as the deuterium

excitation from $\Psi_g(k=0)$ to $\Psi_e(k=\pi/d)$, and assume the same potential barrier V_b for D and H, all other excitation energies are fixed theoretically. Hence, the corresponding protium excitation is expected at 16.6 meV, which compares favorably with the experimental value $\hbar\omega_U = 14.5$ meV. Meanwhile, we have to take a value of $V_b \approx 8$ meV, which is much smaller than the value 102 meV obtained from the first-principles calculation. We note that quantum fluctuations, which are neglected in this approximation, may lower the effective barrier substantially, as discussed in the literature [35]. Further study is required on the influence of fluctuation and self-trapping effects on the dynamics of hydrogen.

In conclusion, we found different excitations of hydrogen in the iron-based superconductor $LaFeAsO_{0.9}D_{0.1}$ using inelastic neutron scattering. We have ascribed the excitations to a quantum rattling, or a band motion of hydrogen, which arises only if the interstitial site has a number of potential minima larger than two. The excitations of hydrogen broaden rapidly when twice the superconducting gap matches the energy of the hydrogen excitation. Assuming a BCS-like temperature dependence of $\Delta(T)$, we estimate a superconducting gap of $\Delta_0 = 7.8$ meV, which agrees with another probe result.

It is evident that the isotropic superconducting gap should be the simplest case for the present probe. Thus, the ion-based superconductors are much more suitable for the analysis than cuprates with nodes in the gap. Moreover, the matching of the superconducting gap with the hydrogen excitation is just fortunate in the iron-based superconductors with appropriate interstitial sites. The hydrogen spectroscopy has a unique feature to scan along the temperature axis with a fixed energy, while most other spectroscopies scan along the energy axis with a fixed temperature. With a further refinement of both measurement and analysis, the hydrogen probe should provide more useful information for clarifying the superconducting gap. Concomitantly, the quantum motion of hydrogen reported in this Rapid Communication deserves a more detailed study in its own right.

We thank K. Yamada and R. Kajimoto for fruitful discussions. This work was supported by MEXT Elements Strategy Initiative to Form Core Research Center and JSPS KAKENHI (Grants No. JP25287081 and No. 16K05434). The neutron and x-ray experiments at J-PARC/MLF and KEK/Photon Factory were performed under user Programs No. 2013S0003, No. 2013A0002(U), No. 2014E0004, No. 2015E0002, and No. 2016S2-004. The DFT calculation has been performed under Large Scale Computer Simulation Program No. T12/13-02, No. 13/14-09, No. 14/15-13, No. 15/16-07, and No. 16/17-18 (FY2012-2015) of KEK. The crystal structure is drawn by using the software VESTA [42].

[1] Y. Kamihara, T. Watanabe, M. Hirano, and H. Hosono, J. Am. Chem. Soc. **130**, 3296 (2008).
[2] J. Paglione and R. L. Greene, Nat. Phys. **6**, 645 (2010).
[3] G. R. Stewart, Rev. Mod. Phys. **83**, 1589 (2011).
[4] H. Hosono and K. Kuroki, Physica C **514**, 399 (2015).
[5] H. Ding, P. Richard, K. Nakayama, K. Sugawara, T. Arakane, Y. Sekiba, A. Takayama, S. Souma, T. Sato, T. Takahashi, Z. Wang, X. Dai, Z. Fang, G. F. Chen, J. L. Luo, and N. L. Wang, Europhys. Lett. **83**, 47001 (2008).
[6] T. Kondo, A. F. Santander-Syro, O. Copie, C. Liu, M. E. Tillman, E. D. Mun, J. Schmalian, S. L. Bud'ko, M. A. Tanatar, P. C. Canfield, and A. Kaminski, Phys. Rev. Lett. **101**, 147003 (2008).
[7] T. Hanaguri, S. Niitaka, K. Kuroki, and H. Takagi, Science **328**, 474 (2010).
[8] T. Y. Chen, Z. Tesanovic, R. H. Liu, X. H. Chen, and C. L. Chien, Nature (London) **453**, 1224 (2008).
[9] R. S. Gonnelli, M. Tortello, D. Daghero, G. A. Ummarino, V. A. Stepanov, and J. S. Kim, Cent. Eur. J. Phys. **7**, 251 (2009).
[10] G. Li, W. Z. Hu, J. Dong, Z. Li, P. Zheng, G. F. Chen, J. L. Luo, and N. L. Wang, Phys. Rev. Lett. **101**, 107004 (2008).
[11] B. Gorshunov, D. Wu, A. A. Voronkov, P. Kallina, K. Iida, S. Haindl, F. Kurth, L. Schultz, B. Holzapfel, and M. Dressel, Phys. Rev. B **81**, 060509(R) (2010).
[12] Y. Fukai, *The Metal-Hydrogen System: Basic Bulk Properties* (Springer, Berlin, 2003).
[13] K. W. Kehr, in *Hydrogen in Metals I: Basic Properties*, edited by G. Alefeld and J. Voelkl (Springer, Berlin, 1978), Vol. 28.
[14] *Hydrogen in Metals III: Properties and Applications*, edited by H. Wipf, Topics in Applied Physics Vol. 73 (Springer, Berlin, 1997).
[15] J. Kondo, Physica B **141**, 305 (1986).
[16] Y. Kagan and N. V. Prokof'ev, in *Quantum Tunnelling in Condensed Media*, edited by Y. Kagan and A. J. Leggett (North-Holland, Amsterdam, 1992), Chap. 2, pp. 37–144.
[17] S. Iimura, S. Matuishi, H. Sato, T. Hanna, Y. Muraba, S. W. Kim, J. E. Kim, M. Takata, and H. Hosono, Nat. Commun. **3**, 943 (2012).
[18] S. Matsuishi, T. Maruyama, S. Iimura, and H. Hosono, Phys. Rev. B **89**, 094510 (2014).
[19] M. Hiraishi, S. Iimura, K. M. Kojima, J. Yamaura, H. Hiraka, K. Ikeda, P. Miao, Y. Ishikawa, S. Torii, M. Miyazaki, I. Yamauchi, A. Koda, K. Ishii, M. Yoshida, J. Mizuki, R. Kadono, R. Kumai, T. Kamiyama, T. Otomo, Y. Murakami, S. Matuishi, and H. Hosono, Nat. Phys. **10**, 300 (2014).
[20] S. Iimura, S. Matsuishi, M. Miyakawa, T. Taniguchi, K. Suzuki, H. Usui, K. Kuroki, R. Kajimoto, M. Nakamura, Y. Inamura, K. Ikeuchi, S. Ji, and H. Hosono, Phys. Rev. B **88**, 060501(R) (2013).
[21] See Supplemental Material at http://link.aps.org/supplemental/10.1103/PhysRevB.99.220505 for INS excitations on the O site, the structure determination, the interstitial sites of hydrogen, the structural optimization and self-trapped state, the peak decomposition of S_{D-F}, and the Mathieu differential equation, which includes Refs. [43–46].
[22] R. Kajimoto, M. Nakamura, Y. Inamura, F. Mizuno, K. Nakajima, S. Ohira-Kawamura, T. Yokoo, T. Nakatani, R. Maruyama, K. Soyama, K. Shibata, K. Suzuya, S. Sato, K. Aizawa, M. Arai, S. Wakimoto, M. Ishikado, S. Shamoto, M. Fujita, H. Hiraka, K. Ohoyama, K. Yamada, and C. H. Lee, J. Phys. Soc. Jpn. **80**, SB025 (2011).
[23] M. Nakamura, R. Kajimoto, Y. Inamura, F. Mizuno, M. Fujita, T. Yokoo, and M. Arai, J. Phys. Soc. Jpn. **78**, 093002 (2009).

[24] Y. Inamura, T. Nakatani, J. Suzuki, and T. Otomo, J. Phys. Soc. Jpn. **82**, SA031 (2013).
[25] A. D. Christianson, M. D. Lumsden, O. Delaire, M. B. Stone, D. L. Abernathy, M. A. McGuire, A. S. Sefat, R. Jin, B. C. Sales, D. Mandrus, E. D. Mun, P. C. Canfield, J. Y. Y. Lin, M. Lucas, M. Kresch, J. B. Keith, B. Fultz, E. A. Goremychkin, and R. J. McQueeney, Phys. Rev. Lett. **101**, 157004 (2008).
[26] S. I. Shamoto, M. Ishikado, A. D. Christianson, M. D. Lumsden, S. Wakimoto, K. Kodama, A. Iyo, and M. Arai, Phys. Rev. B **82**, 172508 (2010).
[27] S. Wakimoto, K. Kodama, M. Ishikado, M. Matsuda, R. Kajimoto, M. Arai, K. Kakurai, F. Esaka, A. Iyo, H. Kito, H. Eisaki, and S. Shamoto, J. Phys. Soc. Jpn. **79**, 074715 (2010).
[28] A. Magerl, A. J. Dianoux, H. Wipf, K. Neumaier, and I. S. Anderson, Phys. Rev. Lett. **56**, 159 (1986).
[29] J. L. Black and P. Fulde, Phys. Rev. Lett. **43**, 453 (1979).
[30] A. Magerl, J. J. Rush, J. M. Rowe, D. Richter, and H. Wipf, Phys. Rev. B **27**, 927 (1983).
[31] D. C. Mattis and J. Bardeen, Phys. Rev. **111**, 412 (1958).
[32] F. Herman and R. Hlubina, Phys. Rev. B **96**, 014509 (2017).
[33] J. P. Perdew, K. Burke, and M. Ernzerhof, Phys. Rev. Lett. **77**, 3865 (1996).
[34] P. G. Sundell and G. Wahnström, Phys. Rev. B **70**, 224301 (2004).
[35] P. G. Sundell, M. E. Björketun, and G. Wahnström, Phys. Rev. B **76**, 094301 (2007).
[36] Y. Iwazaki, T. Suzuki, and S. Tsuneyuki, J. Appl. Phys. **108**, 083705 (2010).
[37] C. P. Flynn and A. M. Stoneham, Phys. Rev. B **1**, 3966 (1970).
[38] Y. Kagan and M. I. Klinger, J. Phys. C **7**, 2791 (1974).
[39] W. Tang, E. Sanville, and G. Henkelman, J. Phys.: Condens. Matter **21**, 084204 (2009).
[40] H. Wipf and K. Neumaier, Phys. Rev. Lett. **52**, 1308 (1984).
[41] A. I. Kolesnikov, V. E. Antonov, S. M. Bennington, B. Dorner, V. K. Fedotov, G. Grosse, J. C. Li, S. F. Parker, and F. E. Wagner, Physica B **263-264**, 421 (1999).
[42] K. Momma and F. Izumi, J. Appl. Crystallogr. **44**, 1272 (2011).
[43] A. Togo and I. Tanaka, Scr. Mater. **108**, 1 (2015).
[44] F. Izumi and K. Momma, Solid State Phenom. **130**, 15 (2007).
[45] I. I. Mazin, M. D. Johannes, L. Boeri, K. Koepernik, and D. J. Singh, Phys. Rev. B **78**, 085104 (2008).
[46] D. J. Singh and M. H. Du, Phys. Rev. Lett. **100**, 237003 (2008).